Prediction of global ionospheric TEC using attention based bidirectional long short-term memory and gated recurrent unit

Shivarudraiah Basavarajaiah[1,2], Raju Garudachar[1]
[1]Department of Electronics Engineering, Jain (deemed-to-be) University, Bengaluru, India
[2]Department Electronics and Communication Engineering, BMS Institute of Technology and Management, Bengaluru, India

Article Info

ABSTRACT

An accurate prediction of ionospheric total electron content (TEC) at the primary stage is essential for applications related to global navigation satellite systems (GNSS) under varying weather conditions. The previous TEC prediction schemes contribute for each time step that increases the prediction time. The eye contact phenomenon establishes a metaphorical connection which intends to capture and emphasize the attention worthy elements in a sequence. This research introduces a deep learning approach which is a combination of attention-based bidirectional long short-term memory and gated recurrent unit (Bi-LSTM GRU) to predict TEC in the ionosphere. Bidirectional LSTM is the better option for achieving durability when combined with a gated recurrent unit (GRU) to predict TEC in the ionosphere. The proposed approach is evaluated with the existing LSTM approach for root mean square error (RMSE) during training and validation. The RMSE while predicting the global ionospheric delay using the existing LSTM for 20 epochs is seen to be 0.004, whereas the existing approach achieves a training error of 0.003.

Corresponding Author:

Shivarudraiah Basavarajaiah
Department of Electronics Engineering, Jain (deemed-to-be) University
Bengaluru, India
Email: shiv2byn@gmail.com

1. INTRODUCTION

The atmosphere of earth is comprised of various layers based on altitude, chemical and thermal characteristics. Among these, the ionosphere is a kind of atmospheric layer that is positioned about 60-1000 km from the surface of the earth [1]. The ionosphere is a significant component that is present in the upper atmosphere of the earth. So, the existence of a large quantity of charged particles considerably affects the propagation of radio waves [2], [3]. The spatiotemporal variations that occur in the ionospheric layer of the atmosphere directly impact on the accuracy of global navigation satellite system (GNSS) for positioning, navigation and other applications. Total electron content (TEC) is one of the significant parameters that is used to describe the ionospheric state [4], [5]. The GNSS broadcast ionospheric delay correction model is designed to offer a global-level description of TEC.

Moreover, the ionospheric delay has complex variations in spatial and temporal dimensionalities which range from several meters to several hundred meters. When the ranges of dimensionalities get increased, the error probability also gets increased and affects the models based on GNSS applications [6]-[9]. The largest naturally occurring error probability of GNSS is rectifiable with the help of broadcasting or empirical models of ionosphere which are generally utilized to diminish the ionospheric delay. The models have the efficiency to achieve better accuracy and meet the needs of the user based on a single frequency and high positioning [8], [9]. The ionospheric time delay is proportional to the ionosphere's TEC. TEC fluctuates

depending on the time of the day, season and year [10]-[12]. GNSS signals enable the monitoring of ionospheric behavior using either ground or space based GNSS receivers [13], [14]. Deep learning techniques characterize ionospheric states using prior ionospheric data under varied space weather situations [15]-[17]. To forecast ionospheric delays, solar and geomagnetic activities are used to classify the ionospheric activity. Ionospheric comportment at low latitudes is highly unpredictable and dynamic. The previous TEC prediction schemes contribute for each time step, increasing the prediction time [18]. The existing approaches are noted as multiple graph cooperative learning neural networks (MGLNN) [19], DenseNet, and swin-transformer prediction head-enabled YOLOv5 with attention mechanism [20], vision transformer (ViT) [21]. Additionally, an effective prediction is not provided by the existing approaches due to maximum error values. As a result, building ionospheric forecasting algorithms requires a great deal of attention [22], [23]. So, this research introduces an effective approach using bidirectional long short-term memory and gated recurrent unit (Bi-LSTM GRU) with an attention mechanism to predict the ionospheric TEC forecasting. Tang et al. [24] introduced a machine learning model referred to as the prophet model which predicted TEC in the ionosphere with the help of a short-term ionospheric prediction model. The training data was obtained from the 15th-order spherical harmonic coefficients, while the predicted coefficients were created using ionospheric TEC forecast map on the basis of solar activity. The proposed approach was applicable based on error correction and offered a stable positioning service for single frequency GNSS. However, the suggested approach was incapable of performing precise predictions with a relatively slight correlation.

Mallika et al. [25] introduced a machine learning algorithm known as Gaussian process regression (GPR) to forecast low-latitude ionospheric conditions. The GPR model was known for its potentiality which was based on kernel based technique with Bayesian rules utilized in forecasting TEC variations in the ionosphere. The suggested approach offered better TEC forecasting performance with small training data, and captured the spatial and temporal patterns with negligible residues. Li et al. [26] introduced an advanced machine-learning approach optimized by genetic algorithm. The suggested approach was a combination of three-dimensional electron density model integrated with meteorology, ionosphere and climate data. The proposed method minimized discrepancies with the capability to enhance its accuracy. However, the error rate was maximal when the simulation took place in a randomized environment. Lin et al. [27] introduced a framework based on spatiotemporal network model to forecast global ionospheric TEC. The suggested spatiotemporal network was comprised of two modules, global spatiotemporal features extraction and regional characteristic correction. In the process of ionospheric prediction, the noise present in the ionospheric TEC data were diminished with the help of the Huber loss function. Reddybattula et al. [28] introduced LSTM to forecast ionospheric TEC through the exploitation of global positioning system (GPS) at low latitudes. The suggested model was trained with the help of the trained data obtained from 2009 to 2017 based on the observed TEC values. An average set of solar and geomagnetic indices were selected with TEC for forecasting the optimistic TEC values. The LSTM architecture was based on the attributes of utilization of maximized filters in the low altitude region. However, TEC forecasting at the regional level had to be considered to improve the refinement at geomagnetic conditions. Zhao et al. [29] introduced an extreme learning machine based spherical harmonic (ELM-SH) model for modeling the ionospheric delay. The SH model was utilized in the process of producing the SH model, whereas the ELM was used in the process of compensating the errors. The ELM-SH algorithm dealt with real-time data based on the stages of training and testing with effective feasibility to model the delay. However, the suggested approach faced problems related to slow convergence and fell into the local extremum.

Iluor and Lu [30] introduced a prediction framework to predict the ionospheric vertical TEC using LSTM and GRU. The performance of LSTM and GRU when predicting GPS-VEC is evaluated, and compared with the performance of multi-layer perceptron (MLP). The GRU has the ability to control the degree of the state which is exposed. However, the usage of LSTM-GRU did not provide effective accuracy due to its poor prediction performance. Chen et al. [31] introduced a multi-step auxiliary prediction model to predict the global ionospheric TEC using deep learning approach. The multi-step auxiliary prediction model had the tendency to predict ionospheric TEC in quiet solar conditions with better generalization ability. However, the prediction error stacking with increased time weakened the multi-step prediction model along with auxiliary algorithm.

Jin and Song [32] developed an hourly updated near real-time Shanghai Astronomical Observatory near real-time global ionospheric map (SHUG). SHUG is based on the hourly estimation as per GNSS data sliding window with spherical harmonic expansion. However, the suggested approach was not able implementable with real time data and TEC forecasting casting. Dabbakuti et al. [33] introduced TEC prediction framework using singular spectrum analysis and autoregressive moving approach. The suggested approach was utilized in signal propagation combined with satellite communication and navigation. SSA had the ability to decompose signals into interpretable and physical components. Nevertheless, the suggested framework was not appropriate for a reliable prediction of ionospheric TEC. Iban and Şentürk [34]

introduced machine learning regression models to predict multiple ionospheric parameters. This research utilized three machine learning approaches namely, decision tree, random forest and support vector machine. The input of the proposed model was evaluated based on peak electron density, critical frequency and TEC. Nonetheless, the forecasting efficiency of the suggested approaches were evaluated only for mid altitude regions where the ionospheric variations are minimal. The significant contributions of this research are listed in the following manner:

a. The Bi-LSTM GRU is introduced to predict TEC in the ionosphere. The Bi-LSTM GRU is highly capable to predict the time forecasting series which is used to predict the TEC in an effective manner.
b. Moreover, the attention mechanism is introduced to cluster critical nodes by including the eye contact phenomenon and aid in effective classification.
c. The performance of the suggested method is evaluated on the basis of various cases of ionospheric delay as a function of frequency for different TEC values, along with the ionospheric delay for solar activities based on intense time and quiet time. Then, the ionospheric delay at different altitude ranges of 300 km and 500 km are studied.

The rest of the research paper is organized in the following way: section 2 describes the proposed method of this research and the experimental results achieved from the proposed method is presented in section 3. Finally, the conclusion of this study is presented in section 4.

2. PROPOSED METHOD

In this research, the TEC in the ionosphere is extracted from the observations of GPS at low latitudes in Bangalore, India. After extracting a decade of data, validation and model development is performed with the help of attention based LSTM-GRU. The input data obtained from the observations of GPS consist of hourly data points from the year 2009 to 2017. The input parameters are comprised of TEC values, and geomagnetic and solar indices. The data which is obtained from GPS is in receiver independent exchange (RINEX) format and is analyzed with the help of the GPS-TEC program. Moreover, the Slant TEC (STEC) units are determined with the help of vertical equivalents (VTEC) by utilizing a single-layered ionospheric model. The input parameters are designed to confirm the 24 h forecast with the signatures of variability for predicting the forecasting in ionosphere using TEC values. The parameters are initialized and the model is trained with around 52,608 datasets, then the dataset is validated for 8,760 samples. During the stage of training, 1000 epochs are utilized with a batch size of 24. The fore mentioned parameters are considered while training the model after which the validation error is evaluated. If the validation error is minimum, the process is terminated, or else the validation error is minimized for last 50 epochs from minimal epoch error. The workflow diagram of the proposed approach is presented in Figure 1.
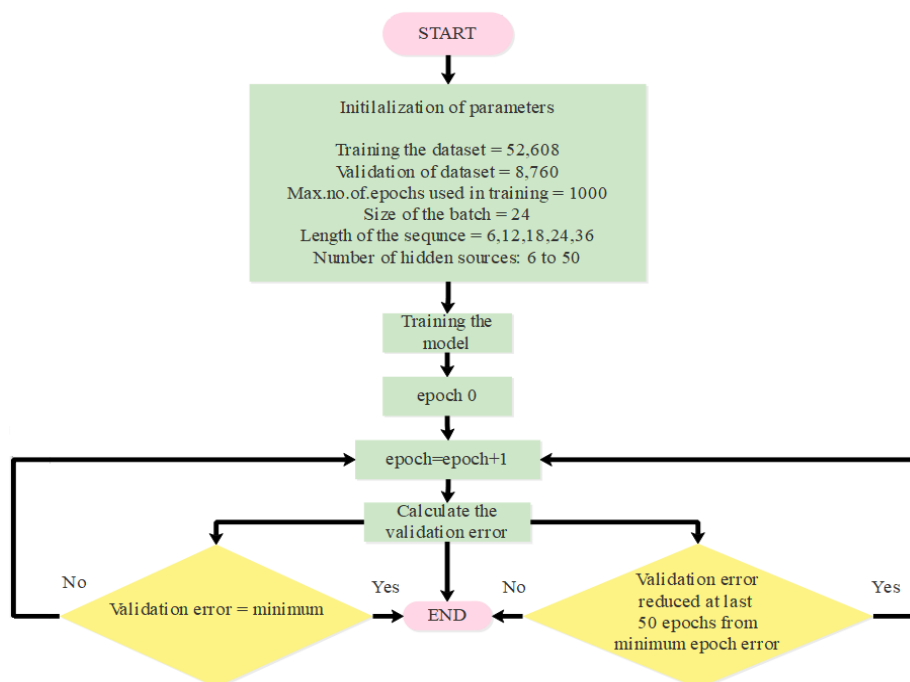

Figure 1. Workflow diagram of the proposed approach

2.1. Attention based BI-LSTM GRU for ionospheric prediction

The RNN separates the order of the data in the form of vectors with a static length. Every individual component is symbolized with a specified instant. As well as the result is influenced for a specified instant over a collection of data from instant $t-1$ which is represented in (1) and (2):

$$h(t) = f(X(t) \times U + h(t-1) \times W + b) \tag{1}$$

$$o(t) = g(h(t) \times V + c) \tag{2}$$

Where, the activation functions denoted as U, W, V represent the weight of the network, while b and c denote the network's deviations. The activation function relies on the network which is represented as f and g. The standard recurrent neural has the ability information related to short-term structure, but not long-term sequence information. The structure of LSTM is covered with input, output, and forget gates. The LSTM feeds the data from input gate and provides it to gate at the output [35]. But, the Bi-LSTM architecture experiences computational complexity $O(W)$ due to the total number of edges present in the network. The Table 1 represents the layer architecture of Bi-LSTM.

Table 1. Representation of layer architecture of Bi-LSTM

Number of input gates	4
Number of output gates	4
Number of forget gates	4
Activation function	Sigmoid, tanh

An optimal dependence is obtained with the help of bidirectional instant in a period of t. So, bidirectional LSTM [36] is the better option to achieve durability when combined with a gated recurrent unit (GRU) [37]. The GRU is comprised of two doors which are an updated door and a reset door represented as z_t and r_t, respectively. The update gate is utilized in the process of supervising knowledge of the previous state, whereas the reset gate is utilized in regulating the degree of transferring knowledge of the previous state. The structural diagram of GRU is depicted in Figure 2.
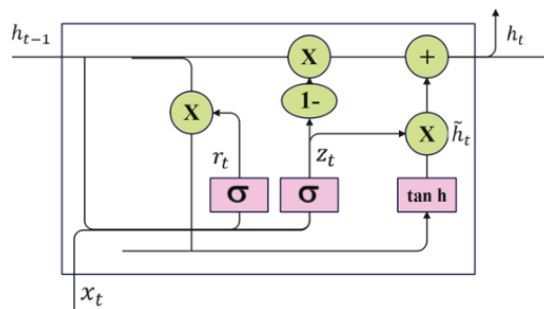

Figure 2. Structural diagram of GRU

Nonetheless, the prediction of ionospheric delay using GRU alone cannot provide a worthy prediction accuracy. To overcome the issues relying on Bi-LSTM and GRU, this research introduces a combination of Bi-LSTM and GRU with an attention mechanism. The mathematical formulations of GRU are given in (3)-(7).

$$r(t) = \sigma(W(r).[h(t-1), x(t)]) \tag{3}$$

$$z(t) = \sigma(W(z).[h(t-1), x(t)]) \tag{4}$$

$$\bar{h}(t) = tanh(W\bar{h}.[r_1 \times h(t-1), x(t)]) \tag{5}$$

$$h(t) = (1 - z(t) \times h(t-1) + z(t) \times \bar{h}(t) \tag{6}$$

$$y(t) = \sigma(W(o).h(t)) \tag{7}$$

2.2. Bi-LSTM GRU with an attention mechanism

The features from Bi-LSTM GRU are combined with attention mechanism to predict the ionospheric delay. The hidden features from the sequential nodes of the Bi-LSTM network are obtained, wherein nodes are utilized to elaborate the meaning of the sequence. The structural diagram of Bi-LSTM GRU with attention mechanism is represented in Figure 3. The effect of significant nodes is improvised with the help of Bi-LSTM layer by embedding the attention layer in it. The attention mechanism is used to cluster critical nodes by including the eye contact phenomenon. The eye contact phenomenon establishes a metaphorical connection which intends to capture and emphasize the attention worthy elements in a sequence. In case of human communication, the eye serves as a non-verbal indication to convey attention. Similarly, a sequence vector is created to represent the crucial node that carries important information within the input sequence. The combination of Bi-LSTM GRU with attention mechanism is used in the representation of sequence. This representation is based on how eye contact enhances the understanding of key inspects in human communications. In (8)-(10) mathematically represent the overall process involved in attention mechanism.

$$u_{it} = tanh(W_n h_{it} + b_n) \tag{8}$$

$$a_{it} = \frac{exp\ (u_{it}^T u_n)}{\sum_t exp\ (u_{it}^T u_n)} \tag{9}$$

$$s_i = \sum_t a_{it} h_{it} \tag{10}$$

Where, the node annotation of MLP and the node level context vector are represented as u_{it} and u_n, respectively. While evaluating the node's significance, the scalar product of u_{it} and u_n is stabilized, and the weight is denoted as a_{it} which is obtained with the help of the softmax function.
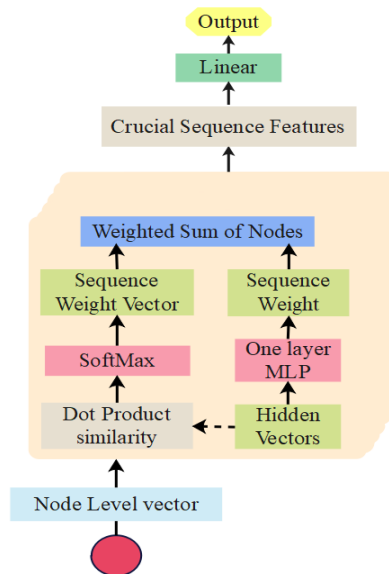

Figure 3. Structural diagrams of Bi-LSTM GRU with an attention mechanism

During the model's training period, the node-level input is evaluated with a contextual vector with related weights. The node level vector is computed based on dot product similarity and fed into the softmax layer. The output from the softmax layer is fed into the sequence of weighted vector. Similarly, the hidden vectors from the dot product similarity are fed into the one-layer MLP, while the sequential weight of hidden vectors are evaluated. The weighted sum of nodes is evaluated based on the dot product similarity and hidden vectors. The significant features are fed into the linear layer which are equal to the number of hidden nodes in the Bi-LSTM layer. In order to assess the efficiency of the suggested approach, an instant evaluation and plotting are retrieved from the community coordinated modeling center (CCMC). IRI-2016 is comprised of a

sub-model system for evaluating the electron density and bottom side thickness. The hourly TEC is evaluated using default options such as NE quick and ABT-2009 correspondingly for the top and bottom side, since they provide better results for equatorial and low-latitude regions.

3. RESULTS AND DISCUSSION

The performance of the suggested approach is evaluated by equating the predicted value of the model with values obtained from GPS-TEC and IRI-2016. IRI is one of the widely recognized models used in the process of evaluating the prediction performance. The IRI-2016 offers information related to forecasting for a specified time and location. The suggested method is estimated by considering the data obtained from 14 incorporated values based on a two-day sequence. The effectiveness of the suggested model is estimated in the system specified with an Intel i7 processor, 8 GB of RAM and windows 10 OS. This section describes the results obtained, alongside evaluating the proposed approach with the existing LSTM model and case studies with various environmental conditions on random days and storm days.

3.1. Performance analysis

The performance of the proposed model is analyzed with the performance of the existing LSTM model deployed in the process of predicting the ionospheric delay and forecasting. The model is analyzed by using the data which is randomly selected from root mean square error (RMSE). The suggested model's performance in prediction of the ionospheric delay is compared with that of the existing LSTM by considering the training and validation error for different epochs. Table 2 presents the RMSE that occurs while training and validation of the proposed Bi-LSTM GRU with the state-of-the-art techniques namely, LSTM, Bi-LSTM, and GRU.

Table 2. Evaluation of RMSE between LSTM and Bi-LSTM GRU

| Epochs | RMSE | | | | | | | |
| | LSTM | | Bi-LSTM | | GRU | | Bi-LSTM GRU | |
	Training error	Validation error	Training error	Validation error	Training error	Validation error	Training error	Validation error
1	0.05	0.05	0.04	0.04	0.05	0.04	0.03	0.04
5	0.004	0.004	0.003	0.003	0.04	0.03	0.002	0.012
10	0.003	0.041	0.002	0.003	0.004	0.005	0.023	0.018
15	0.003	0.004	0.005	0.003	0.004	0.004	0.028	0.020
20	0.004	0.004	0.004	0.005	0.004	0.006	0.003	0.001

The results from Table 2 show that the proposed approach achieves a minimal error rate when compared with the existing LSTM, Bi-LSTM, and GRU architectures for ionospheric prediction. For example, the validation error of the proposed approach for 20 epochs is 0.001, whereas the validation error of LSTM, Bi-LSTM and GRU is 0.004, 0.005 and 0.006, respectively. The superior result of the proposed approach is due to the combination of Bi LSTM and GRU with an attention mechanism, thereby improving the clustering ability and providing a better prediction performance. The graphical representation for the evaluation of RMSE based on the training error and validation error is represented in Figure 4.
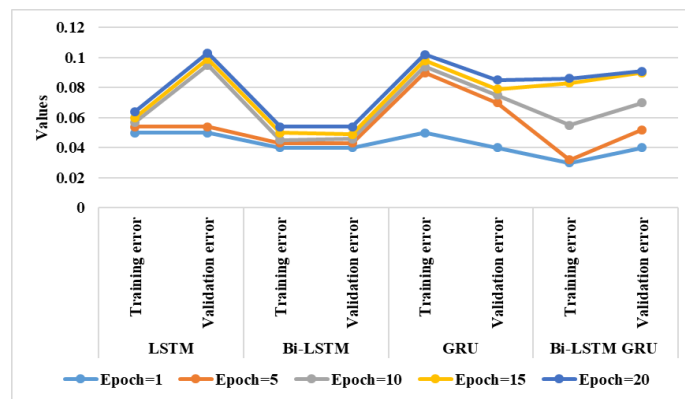

Figure 4. Graphical representation for evaluation of RMSE

Figure 5 presents TEC (TECU) forecasting of the GPS, IRI, LSTM, and the proposed approach that are evaluated for random days in the year 2018. It is observed that the Bi-LSTM GRU predicts the hourly values based on GPS observations, whereas the IRI TEC estimates for the days considered in a randomized manner. Figure 5 exhibits that the suggested Bi-LSTM GRU with attention mechanism accomplishes better results for predicting TEC in the ionosphere for random days. Here, $1 \text{ TECU} = 1 \times 10^{16} \frac{electrons}{m^2}$. Figure 6 evidences that the suggested Bi-LSTM GRU with attention mechanism accomplishes better results for predicting the TEC in the ionosphere on storm days in the year 2018.
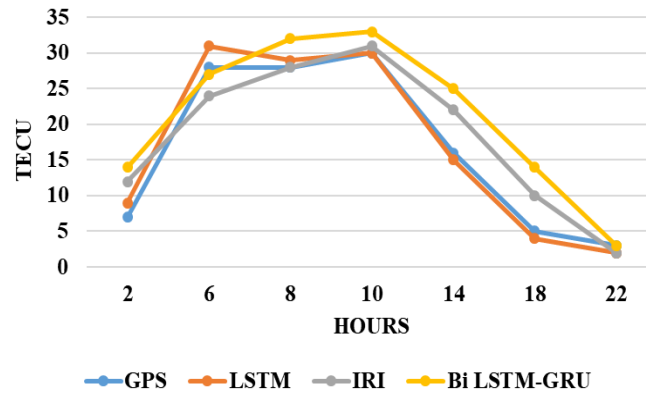

Figure 5. Graphical representations for TEC prediction using different approaches on a random day of the year
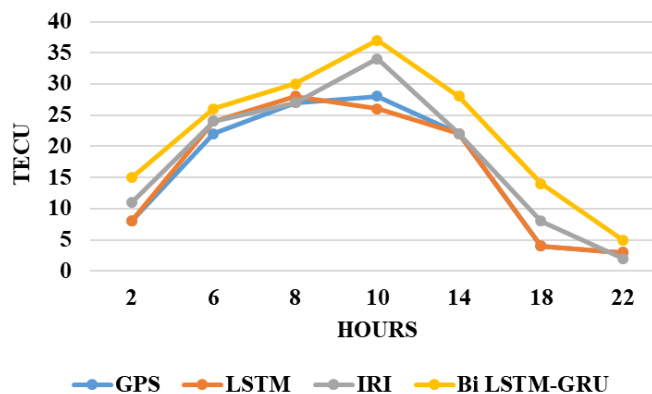

Figure 6. Graphical representations for TEC prediction using different approaches on a storm day of the year

3.2. Case studies for the proposed method

Since this is the first research where the proposed approach is evaluated with real time dataset for the prediction of ionospheric delay, the papers with similar datasets are not available. So, case studies are performed based on ionospheric delay as a function of frequency for different TEC values, for intense and quiet solar activities, and as a function of frequency for different altitude ranges, with 300 km as the lowest range and 500 km as the highest range.

3.2.1. Case 1: ionospheric delay as a function of frequency for different TEC values

In case 1, the proposed Bi-LSTM GRU model is evaluated for different TEC values of 1e15 (0.1 TECU), 5e15 (0.5 TECU), and 1e16 (1 TECU). The result is taken as frequency (GHz) with ionosphere delay (ms) to evaluate the performance of the proposed method. Figure 7 presents the graph between ionospheric delay and frequency ranges of 1 GHz to 10 GHz. The results from Figure 7 show that the ionospheric delay increases when the value of TEC increases, proving to be directly proportional to one another. For the frequency of 2 GHz, the proposed approach achieves a delay of 0.25 ms for TEC of 1e15 (0.1 TECU), and further a delay of 1.1 ms for TEC of 5e15 (0.5 TECU).

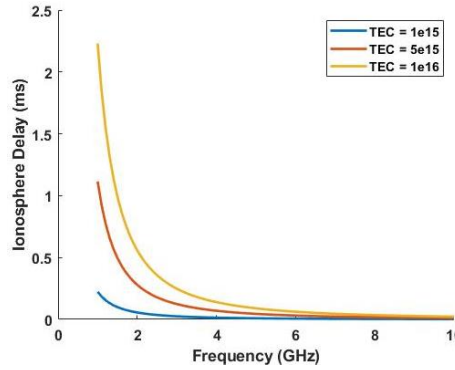Figure 7. Evaluation of ionospheric delay for different TEC values

3.2.2. Case 2: ionospheric delay for solar activities

In case 2, the variation of ionospheric TEC is considered based on the effect of solar activity. The correlation between the solar sunspot and average solar flux F10.7 is considered for 15 days, before and after the extra-large flare is used to make the evaluation. The substantial positive link between the number of solar sunspots, the solar F10.7 index, and the temperature before and after this flare burst. The influence of solar activity on TEC is around 2 days delayed. The solar activity's influence on global ionospheric TEC is not synchronized. There is a one-day delay from high to low latitudes, while the influence on low latitudes is significantly stronger than on the middle and high latitudes. In general, solar activity is the primary cause of ionospheric TEC variation, but other relevant causes are also possible to exist locally [38]. A violent solar storm that swept over earth on February 27th, 2023, forced SpaceX to postpone a Starlink launch from Florida, and momentarily hampered operations of numerous Canadian oil rigs due to faulty GPS signals. When a massive numbers of charged solar particles reach the earth, their interactions with the upper atmosphere cause the atmosphere to inflate. When this occurs, the density of gases at higher altitudes rises, causing the spacecraft to encounter a increased drag. Because the SpaceX launches Starlink vessels at very low altitudes and then uses the satellite's onboard engine to increase its orbit, the extra drag proves too much for the doomed spacecraft. The ionospheric delay for different solar activities of 0.8, 1.2, 1.5, 1.7, and 2 with solar intense and solar quiet time are graphically illustrated in Figure 8.

The outcomes from Figure 8 prove that the proposed method is robust for varying frequency ranges from 1 GHz to 10 GHz. For instance, when the frequency is 1 GHz, the ionospheric delay is 3.5 ms for solar activity of 0.8. Similarly, for solar activity of 2, the ionospheric delay is 8.9 ms. While evaluating the ionospheric delay for quiet time for a frequency of 1 GHz, the ionospheric delay is 0.9 ms for solar activity of 0.8, whereas for solar activity of 2, the ionospheric delay is 2.1 ms.
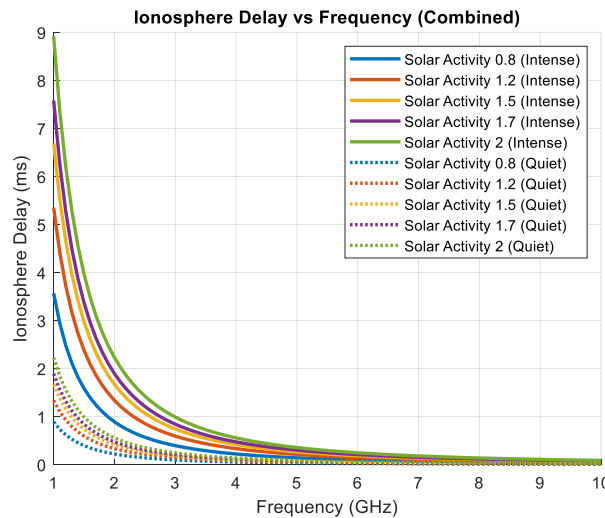

Figure 8. Ionospheric delay of solar activities based on intense and quiet time

3.2.3. Case 3: ionospheric delay at different frequencies for an altitude of 300 km

The results from Figure 9 demonstrate the ionospheric delay of the proposed approach for different weather conditions such as summer, winter and rainy, at an altitude of 300 km. The outcomes are taken as frequency (GHz) with ionosphere delay (ms) to evaluate the performance of the proposed method. For a frequency of 2 GHz, the ionospheric delay in winter is 0.6201 ms, the ionospheric delay in rainy season is 0.6203 ms, and 0.6204 ms in summer season.
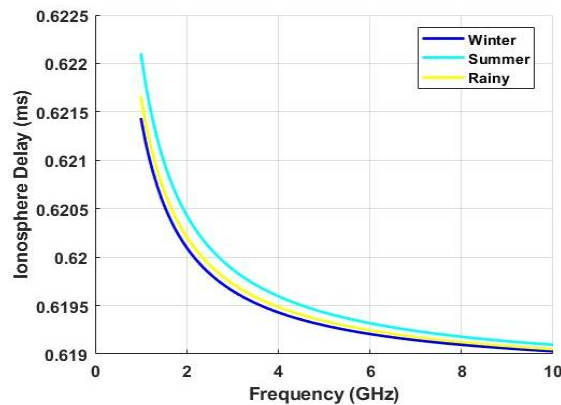

Figure 9. Evaluation of ionospheric delay for different frequencies for an altitude of 300 km

3.2.4. Case 4: ionospheric delay at different frequencies for an altitude of 500 km

The outcomes from Figure 10 demonstrate the ionospheric delay of the proposed approach for different weather conditions such as summer, winter and rainy, at an altitude of 500 km. The results are taken as frequency (GHz) with ionosphere delay (ms) to assess the performance of the proposed method. For a frequency of 2 GHz, the ionospheric delay in winter is 0.6207 ms, the ionospheric delay in rainy season is 0.6209 ms, and 0.6212 ms in the summer season.
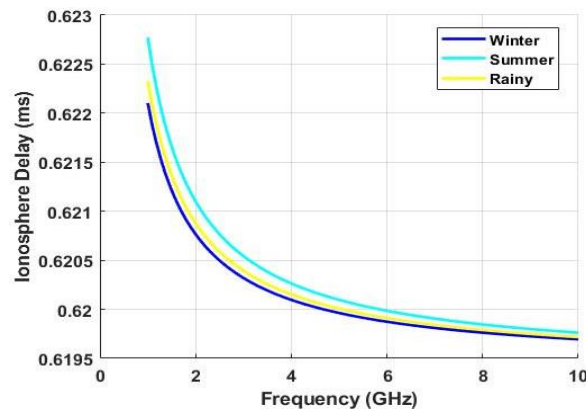

Figure 10. Evaluation of ionospheric delay for different frequencies for an altitude of 500 km

3.2.5. Case 5: delay comparison between ionosphere and troposphere regions at different time zones from different channels

In case 5, the proposed approach is evaluated with real time data on 8th July, 2023 obtained from the IRNSS receiver. The geo location of the data captured are noted as: Latitude: 12.38 ^{0}N, Longitude: 77.26^{0}E (JAIN Global Campus, Bengaluru). The channels considered for comparison are 2, 3, 6, and 9 which are based on two time zones from 3 AM–5 AM and 12 PM–15 PM. The outcomes attained while evaluating the proposed approach for different time zones from 3 AM–5 AM and 12 PM–15 PM for different channels are presented in Table 3.

The results from Table 3 show the results of the proposed approach for different channels and time zones. The results are taken when the solar activity is minimal (i.e., 3 AM–5 AM), as well as when the solar

activity is high (i.e., 12 PM–15 PM). For instance, the ionospheric delay is 0.095 ms for channel 9, and the tropospheric delay is 0.012 ms for channel 9 in the time zone of 3 AM-5 AM. Similarly, for the time zone between 12 PM-15 PM, the ionospheric delay is 0.114 for channel number 9, whereas for the same channel number 9, the tropospheric delay is 0.009 ms. As the ionosphere lies in the range of 50-400 km from the earth's surface, it is exposed to a large quantity of solar intenses, while the troposphere is the primary layer from the surface of the earth which lies around 0-10 km from the earth's surface. Figure 11 shows the graphical illustration of both ionospheric delay and tropospheric delay for two time ranges from 3 AM-5 AM and 12 PM-15 PM.

Table 3. Evaluation of ionospheric delay and the tropospheric delay for different channels

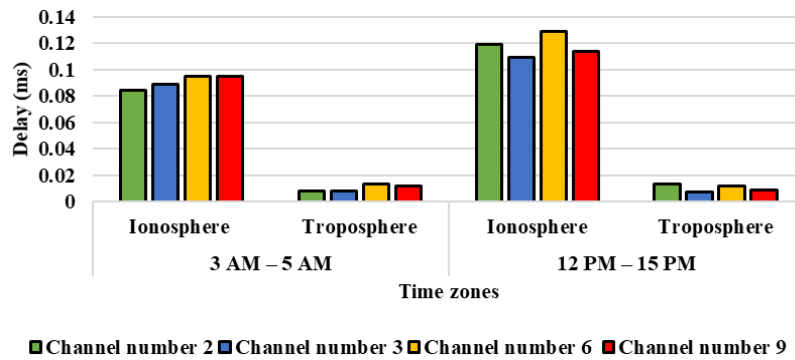| Channels	3 AM–5 AM		12 PM–15 PM	
	Ionospheric delay (ms)	Tropospheric delay (ms)	Ionospheric delay (ms)	Tropospheric delay (ms)
2	0.084	0.008	0.119	0.013
3	0.089	0.008	0.109	0.007
6	0.095	0.013	0.129	0.012
9	0. 095	0.012	0.114	0.009

Figure 11. Comparison of ionospheric delay and tropospheric delay for different channels at different time zones from 3 AM-5 AM and 12 PM-15 PM

3.3. Ablation study

This section presents the ablation study where the efficiency of the proposed Bi-LSTM GRU is assessed based on the presence and absence of attention mechanism. The Table 4 presents the results achieved while evaluating the proposed approach based on presence and absence of attention mechanism. The results from the Table 4 evidence that the Bi-LSTM achieves better performance by acquiring minimal RMSE. The different epochs count are 1, 5, 10, 15, and 20. The RMSE during the training of Bi-LSTM GRU without attention mechanism for 20 epochs is 0.004, whereas the Bi-LSTM GRU with attention mechanism achieves 0.003. Thus, the inclusion of attention mechanism helps to minimize the error rate while predicting TEC in the ionosphere. The attention mechanism has the ability to adapt itself to the varying length of input sequence and to the length of input sequence, thereby aiding for preferable prediction results.

Table 4. Evaluation of RMSE for Bi-LSTM GRU with and without attention mechanism

	RMSE			
Epochs	Bi-LSTM GRU without attention mechanism		Bi-LSTM GRU with attention mechanism	
	Training error	Validation error	Training error	Validation error
1	0.04	0.05	0.03	0.04
5	0.05	0.03	0.002	0.012
10	0.005	0.005	0.023	0.018
15	0.006	0.005	0.028	0.020
20	0.004	0.006	0.003	0.001

4.   CONCLUSION

Deep learning is useful for solving problems by detecting patterns and relationships in previous data. In a mathematical approach, computer systems learn by example and extract relevant information from

a vast set of historical data. It often comprises a vast amount of information that spans as many criteria as feasible and the attention-based Bi-LSTM GRU is deployed to predict the TEC in the ionosphere. This research introduces a deep learning approach which is a combination of attention-Bi-LSTM GRU to predict TEC in the ionosphere. Bidirectional LSTM is a robust option to achieve durability when combined with a GRU to predict TEC in the ionosphere. Likewise, Bi-LSTM is a sturdy option to achieve durability when combined with a GRU for the same. The proposed approach is contrasted against the existing LSTM approach for RMSE during training and validation. The efficiency of the proposed approach is analysed with the help of case studies of ionospheric delay for different TEC and solar activities based on intense and quiet time. Moreover, the ionospheric delay for altitude ranges between the lowest altitude of 300 km and the highest altitude of 500 km is evaluated. The training error of Bi-LSTM GRU without attention mechanism for 20 epochs is 0.004 whereas the proposed approach achieved a training error of 0.003. The future work of this research will be based on predicting the ionospheric delay by changing the values of the activation function. Moreover, the model experiences overfitting when the dataset is not large enough, and this can be rectified using regularization techniques.

ACKNOWLEDGEMENTS

REFERENCES

[1]   J. Tang, Z. Zhong, M. Ding, D. Yang, and H. Liu, "Forecast of Ionospheric TEC Maps Using ConvGRU Deep Learning over China," *IEEE Journal of Selected Topics in Applied Earth Observations and Remote Sensing*, vol. 17, pp. 3334–3344, 2024, doi: 10.1109/JSTARS.2024.3349392.
[2]   Y. Yuan, N. Wang, Z. Li, and X. Huo, "The BeiDou global broadcast ionospheric delay correction model (BDGIM) and its preliminary performance evaluation results," *Navigation*, vol. 66, no. 1, pp. 55–69, 2019, doi: 10.1002/navi.292.
[3]   L. Li et al., "Spatiotemporal Prediction of Ionospheric Total Electron Content Based on ED-ConvLSTM," *Remote Sens.*, vol. 15, no. 12, p. 3064, 2023, doi: 10.3390/rs15123064.
[4]   N. Wang, Z. Li, Y. Yuan, and X. Huo, "BeiDou Global Ionospheric delay correction Model (BDGIM): performance analysis during different levels of solar conditions," *GPS Solutions*, vol. 25, p. 97, 2021, doi: 10.1007/s10291-021-01125-y.
[5]   W. Huang, Y. Chen, T. Xin, H. Xie, L. Huang, and L. Ji, "Ionospheric prediction algorithm and its application in low-latitude regions based on the physically constrained polynomial model," *J. Phys. Conf. Ser., 2023 5th International Conference on Energy Systems and Electrical Power*, Changsha, China, vol. 2584, p. 012136, 2023, doi: 10.1088/1742-6596/2584/1/012136.
[6]   J. Cheng, C. Jiang, C. Jia, J. Ding, H. Li, and B. Qi, "Evaluation of Ionospheric Delay Extraction Model Using Dual-Frequency Multisystem Observations," *IEEE Sensors Journal*, vol. 23, no. 14, pp. 16197–16209, 2023, doi: 10.1109/JSEN.2023.3278095.
[7]   C. Zhang, Y. Dang, X. Wang, J. Quan, and Z. Yu, "A Real-Time Cycle Slip Detection and Repair Method Based on Ionospheric Delay Prediction for Undifferenced Triple-Frequency BDS Signals," *IEEE Access*, vol. 9, pp. 69999–70013, 2021, doi: 10.1109/ACCESS.2021.3078325.
[8]   J. Wang, Q. Yu, Y. Shi, and C. Yang, "A Prediction Method of Ionospheric hmF2 Based on Machine Learning," *Remote Sens.*, vol. 15, no. 12, p. 3154, 2023, doi: 10.3390/rs15123154.
[9]   I. Srivani, G. S. V. Prasad, and D. V. Ratnam, "A Deep Learning-Based Approach to Forecast Ionospheric Delays for GPS Signals," *IEEE Geosci. Remote Sens. Lett.*, vol. 16, no. 8, pp. 1180–1184, 2019, doi: 10.1109/LGRS.2019.2895112.
[10]   Y. Yuan, G. Xia, X. Zhang, and C. Zhou, "Synthesis-Style Auto-Correlation-Based Transformer: A Learner on Ionospheric TEC Series Forecasting," *Space Weather*, vol. 21, no. 10, p. e2023SW003472, 2023, doi: 10.1029/2023SW003472.
[11]   L. Zhao, J. Douša, and P. Václavovic, "Accuracy Evaluation of Ionospheric Delay from Multi-Scale Reference Networks and Its Augmentation to PPP during Low Solar Activity," *ISPRS Int. J. Geo-Inf.*, vol. 10, no. 8, p. 516, 2021, doi: 10.3390/ijgi10080516.
[12]   A. Ruwali, A. J. S. Kumar, K. B. Prakash, G. Sivavaraprasad, and D. V. Ratnam, "Implementation of Hybrid Deep Learning Model (LSTM-CNN) for Ionospheric TEC Forecasting Using GPS Data," *IEEE Geosci. Remote Sens. Lett.*, vol. 18, no. 6, pp. 1004–1008, 2021, doi: 10.1109/LGRS.2020.2992633.
[13]   J. Chen and Y. Gao, "Real-Time Ionosphere Prediction Based on IGS Rapid Products Using Long Short-Term Memory Deep Learning," *NAVIGATION: Journal of the Institute of Navigation*, vol. 70, no. 2, 2023, doi: 10.33012/navi.581.
[14]   W. Li et al., "A satellite-based method for modeling ionospheric slant TEC from GNSS observations: Algorithm and validation," *GPS Solutions*, vol. 26, p. 14, 2022, doi: 10.1007/s10291-021-01191-2.
[15]   D. Yang and H. Fang, "Forecasting of global ionospheric TEC using a deep learning approach," *GPS Solutions*, vol. 27, p. 74, 2023, doi: 10.1007/s10291-023-01413-9.
[16]   K. Su and S. Jin, "Three Dual-Frequency Precise Point Positioning Models for the Ionospheric Modeling and Satellite Pseudorange Observable-Specific Signal Bias Estimation," *Remote Sens.*, vol. 13, no. 24, p. 5093, 2021, doi: 10.3390/rs13245093.
[17]   N. Shenvi and H. Virani, "Forecasting of Ionospheric Total Electron Content Data Using Multivariate Deep LSTM Model for Different Latitudes and Solar Activity," *J. Electr. Comput. Eng.*, vol. 2023, p. 2855762, 2023, doi: 10.1155/2023/2855762.
[18]   X. Ren, P. Yang, H. Liu, J. Chen, and W. Liu, "Deep learning for global ionospheric TEC forecasting: Different approaches and validation," *Space Weather*, vol. 20, no. 5, p. e2021SW003011, 2022, doi: 10.1029/2021SW003011.
[19]   B. Jiang, S. Chen, B. Wang, and B. Luo, "MGLNN: Semi-supervised learning via multiple graph cooperative learning neural networks," *Neural Networks*, vol. 153, p. 204–214, 2022, doi: 10.1016/j.neunet.2022.05.024.
[20]   A. M. Roy and J. Bhaduri, "DenseSPH-YOLOv5: An automated damage detection model based on DenseNet and Swin-Transformer prediction head-enabled YOLOv5 with attention mechanism," *Adv. Eng. Inf.*, vol. 56, p. 102007, 2023, doi: 10.1016/j.aei.2023.102007.

[21] S. Jamil and A. M. Roy, "An efficient and robust phonocardiography (pcg)-based valvular heart diseases (vhd) detection framework using vision transformer (vit)," *Comput. Biol. Med.*, vol. 158, p. 106734, 2023, doi: 10.1016/j.compbiomed.2023.10673

[22] P. Xiong, C. Long, H. Zhou, X. Zhang, and X. Shen, "GNSS TEC-based earthquake ionospheric perturbation detection using a novel deep learning framework," *IEEE J. Sel. Top. Appl. Earth Obs. Remote Sens.*, vol. 15, pp. 4248–4263, 2022, doi: 10.1109/JSTARS.2022.3175961.

[23] C. Borries, A. A. Ferreira, G. Nykiel, and R. A. Borges, "A new index for statistical analyses and prediction of travelling ionospheric disturbances," *J. Atmos. Sol. Terr. Phys.*, vol. 247, p. 106069, 2023, doi: 10.1016/j.jastp.2023.106069.

[24] J. Tang, Y. Li, D. Yang, and M. Ding, "An approach for predicting global ionospheric TEC using machine learning," *Remote Sens.*, vol. 14, no. 7, p. 1585, 2022, doi: 10.3390/rs14071585.

[25] L. I. Mallika, D. V. Ratnam, S. Raman, and G. Sivavaraprasad, "Machine learning algorithm to forecast ionospheric time delays using Global Navigation satellite system observations," *Acta Astronaut.*, vol. 173, pp. 221–231, 2020, doi: 10.1016/j.actaastro.2020.04.048

[26] W. Li, D. Zhao, C. He, A. Hu, and K. Zhang, "Advanced machine learning optimized by the genetic algorithm in ionospheric models using long-term multi-instrument observations," *Remote Sens.*, vol. 12, no. 5, p. 866, 2020, doi: 10.3390/rs12050866.

[27] X. Lin *et al*., "A spatiotemporal network model for global ionospheric TEC forecasting," *Remote Sens.*, vol. 14, no. 7, p. 1717, 2022, doi: 10.3390/rs14071717.

[28] K. D. Reddybattula *et al*., "Ionospheric TEC forecasting over an Indian low latitude location using long short-term memory (LSTM) deep learning network," *Universe*, vol. 8, no. 11, p. 562, 2022, doi: 10.3390/universe8110562.

[29] T. Zhao, S. Pan, W. Gao, Z. Qing, X. Yang, and J. Wang, "Extreme learning machine-based spherical harmonic for fast ionospheric delay modelling," *J. Atmos. Sol. Terr. Phys.*, vol. 216, p. 105590, 2021, doi: 10.1016/j.jastp.2021.105590.

[30] K. Iluore and J. Lu, "Long short-term memory and gated recurrent neural networks to predict the ionospheric vertical total electron content," *Adv. Space Res.*, vol. 70, no. 3, pp. 652–665, 2022, doi: 10.1016/j.asr.2022.04.066.

[31] Z. Chen, W. Liao, H. Li, J. Wang, X. Deng, and S. Hong, "Prediction of global ionospheric TEC based on deep learning," *Space Weather*, vol. 20, no. 4, p. e2021SW002854, 2022, doi: 10.1029/2021SW002854.

[32] X. Jin and S. Song, "Near real-time global ionospheric total electron content modeling and nowcasting based on GNSS observations," *Journal of Geodesy*, vol. 97, no. 3, p. 27, 2023, doi: 10.1007/s00190-023-01715-3.

[33] J. R. K. K. Dabbakuti, M. Yarrakula, S. K. Panda, P. Jamjareegulgarn, and M. A. Haq, "Total electron content prediction using singular spectrum analysis and autoregressive moving average approach," *Astrophys. Space Sci.*, vol. 367, no. 1, p. 8, 2022, doi: 10.1007/s10509-021-04036-z.

[34] M. C. Iban and E. Şentürk, "Machine learning regression models for prediction of multiple ionospheric parameters," *Adv. Space Res.*, vol. 69, no. 3, pp. 1319–1334, 2022, doi: 10.1016/j.asr.2021.11.026.

[35] G. S. Alsoruji, A. M. Sadoun, M. A. Elaziz, M. A. Al-Betar, A. W. Abdallah, and A. Fathy, "On the prediction of the mechanical properties of ultrafine grain Al-TiO2 nanocomposites using a modified long-short term memory model with beluga whale optimizer," *J. Mater. Res. Technol.*, vol. 23, pp. 4075–4088, 2023, doi: 10.1016/j.jmrt.2023.01.212.

[36] H. Tabrizchi, J. Razmara, and A. Mosavi, "Thermal prediction for energy management of clouds using a hybrid model based on CNN and stacking multi-layer bi-directional LSTM," *Energy Rep.*, vol. 9, pp. 2253–2268, 2023, doi: 10.1016/j.egyr.2023.01.032.

[37] S. Reza, M. C. Ferreira, J. J. M. Machado, and J. M. R. Tavares, "A customized residual neural network and bi-directional gated recurrent unit-based automatic speech recognition model," *Expert Syst. Appl.*, vol. 215, p. 119293, 2023, doi: 10.1016/j.eswa.2022.119293.

[38] L. Yongtao, L. Jianwen, D. Taogao, and P. Peng, "Influence of Solar Activity on Ionospheric TEC Change," *Chinese Journal of Space Science*, vol. 38, no. 6, pp. 847–854, 2018, doi: 10.31401/SunGeo.2019.02.05.

BIOGRAPHIES OF AUTHORS

Shivarudraiah Basavarajaiah holds B.E. degree in Electronics and Communication Engineering and M.Tech. degree in VLSI Design and Embedded System from Visvesvaraya Technological University, Bangalore, Karnataka, India. His research interests are Ionosphere study and analysis, VLSI design, embedded systems, and image processing. He can be contacted at email: shiv2byn@gmail.com.

Raju Garudachar holds degrees of B.E. (Electronics-Bangalore University), M.E. (Electronics–BITS, Pilani) and Ph.D. (Electronics and Computer Engineering–University of Kansas, USA). He worked in ISRO for 40 years (1972-2012) on topics related to satellite systems and payloads, microwave systems, satellite communication, radar and radiometry, at the Space Applications Centre (SAC), Ahmedabad and the ISRO Satellite Centre (ISAC), Bangalore. The last responsibility at ISRO was as Project Director for an Indo-French (ISRO-CNES)–Megha-Tropiques Climate Satellite. As a part of Ph.D. degree in USA, he developed a Ice-Penetrating Radar and conducted measurements in Antarctica in 1986 and 87. He can be contacted at email: g.raju@jainuniversity.ac.in.